crystals

MDPI

Article

Spatial Anisotropy of Photoelasticity Determined by Path Difference in $Ba_3TaGa_3Si_2O_{14}$ Crystals

Natalia Demyanyshyn [1], Oleh Buryy [2,*], Bohdan Mytsyk [1], Pavlo Solomenchuk [2], Oleksandr Lishchuk [2] and Anatoliy Andrushchak [2]

[1] Karpenko Physico-Mechanical Institute, 5 Naukova St., 79601 Lviv, Ukraine; nmdem@ukr.net (N.D.); mytsykb@ukr.net (B.M.)
[2] Lviv Polytechnic National University, 12 Bandery St., 79046 Lviv, Ukraine; pavlo.solomenchuk@gmail.com (P.S.); oleksandr.o.lishchuk@lpnu.ua (O.L.); anatolii.s.andrushchak@lpnu.ua (A.A.)
* Correspondence: oleh.a.buryi@lpnu.ua

Abstract

The elastic and photoelastic coefficients of $Ba_3TaGa_3Si_2O_{14}$ (BTGS) crystals were determined by the quantum–mechanical calculation technique. Based on these data, extreme piezo-optic surfaces $\pi'^{\circ}{}_{km}$ were constructed, which describe the change in the path difference in light beams in the crystal under the influence of mechanical stress. The results for BTGS crystals are compared with the ones for other crystals of the langasite group ($La_3Ga_5SiO_{14}$, $Ca_3Ga_2Ge_4O_{14}$, $Ca_3TaGa_3Si_2O_{14}$ and $Ca_3NbGa_3Si_2O_{14}$). The global maxima of the $\pi'^{\circ}{}_{km}$ surfaces for BTGS crystals significantly exceed the ones for the other crystals mentioned above and, accordingly, BTGS crystals can be suitable for use in polarization-optic light modulators and devices based on them. The acousto-optic efficiency of BTGS crystals was evaluated. The correlations between the magnitude of the piezo- and elasto-optic coefficients and the parameters of the unit cell of the studied crystals were determined.

Keywords: piezo-optic effect; elasto-optic effect; quantum–mechanical calculation; extreme surfaces; acousto-optic efficiency

check for updates

Academic Editor: Lili Li

Received: 9 June 2025
Revised: 24 July 2025
Accepted: 28 July 2025
Published: 31 July 2025

Citation: Demyanyshyn, N.; Buryy, O.; Mytsyk, B.; Solomenchuk, P.; Lishchuk, O.; Andrushchak, A. Spatial Anisotropy of Photoelasticity Determined by Path Difference in $Ba_3TaGa_3Si_2O_{14}$ Crystals. *Crystals* **2025**, *15*, 708. https://doi.org/10.3390/cryst15080708

Copyright: © 2025 by the authors. Licensee MDPI, Basel, Switzerland. This article is an open access article distributed under the terms and conditions of the Creative Commons Attribution (CC BY) license (https://creativecommons.org/licenses/by/4.0/).

1. Introduction

Sensitive elements of optical modulating devices are, as a rule, bulk crystalline materials. The number of photoelastic materials that have been used in practice includes few crystals, so the task of finding new effective materials for controlling laser radiation is relevant.

Interest in crystals of the langasite group [1–6] is due to the fact that they reveal a unique combination of various physical properties. For instance, the temperature stability of physical characteristics, in particular elastic [7,8], as well as a large piezoelectric effect and a high coefficient of electromechanical coupling (e.g., the value of the piezoelectric coefficient d_{11} of langasite group crystals is in the range of 4…7 pC/N [9–11], that is 2…3 times higher than in quartz crystals [9])—makes them a popular material for development of acoustoelectronic devices [6]. In particular, they are used in pressure and detonation sensors, resonators in tunable generators, substrates of thermostable slices for acoustoelectronic filters on surface and bulk acoustic waves, Q-switches, as well as temperature-stable broadband monolithic filters used in mobile communication systems [12–14]. Because of a high optical damage threshold of ~1 GW/cm^2 [15], these crystals can be used as sensitive elements in acousto-optical converters. The optical properties of crystals of the LGS group

have also been widely studied, see, e.g., works [1,4,9,13,16,17]. However, the photoelastic properties of these crystals were not investigated until our first papers [18–20]. In our previous works, the piezo-, elasto- and acousto-optical properties of several representatives of this group were experimentally studied: crystals of langasite $La_3Ga_5SiO_{14}$ (LGS) [18] and calcium halogermanate $Ca_3Ga_2Ge_4O_{14}$ (CGG) [20], which have a disordered structure (see [21]), and crystals of catangasite $Ca_3TaGa_3Si_2O_{14}$ (CTGS) [19] with an ordered structure (see [22]). However, for most crystals of the LGS group (for a list of these crystals, see, e.g., [21,22]), the piezo-optic effect (POE), the elasto-optic effect (ELOE), and the acousto-optic efficiency have not been studied. It is these effects that are interesting from the point of view of the application of crystals of the LGS group, because of the stability of physical characteristics, high optical quality of the crystals, their high mechanical strength [19,20], and transparency in the deep ultraviolet region (up to ~250 nm [1,9,20]).

Since it is problematic to experimentally study a large number of crystals by the laborious interferometric method [19,20,23], in paper [24] the photoelastic (piezo- and elasto-optic) coefficients of ordered CTGS and $Ca_3NbGa_3Si_2O_{14}$ (CNGS) crystals were calculated by the quantum–mechanical technique. The calculation results for CTGS crystals [24] agree well with the experimental data [19]. Therefore, in this paper, the elastic, piezo- and elasto-optic coefficients of ordered batangasite $Ba_3TaGa_3Si_2O_{14}$ (BTGS) crystals were calculated in a similar way. Based on these results, the spatial anisotropy of photoelasticity effects can be studied by the methods of indicative or extreme surfaces, see, e.g., [25–28]. Here the extreme surfaces describing the change in the path difference of the orthogonally polarized light beams

$$\delta\Delta_k = \delta(\Delta n_k \cdot d_k) \quad (1)$$

under the influence of mechanical stress σ_m is constructed and the maximum values of this effect are found (here Δn_k is the birefringence of the crystal, d_k is the thickness of the sample in the direction of light propagation). The results obtained for BTGS crystal are compared with similar ones for LGS, CTGS, CNGS and CGG.

2. Material and Method for Determining Photoelastic Coefficients

BTGS crystals were chosen for calculating the piezo-optic coefficients (POCs) π_{im} and elasto-optic coefficients (ELOCs) p_{ik} because their photoelastic properties have not been elucidated yet. In addition, because of the high refractive indices ($n_i \approx 2$ [29]), which are decisive for the value of the acousto-optic figure-of-merit M_2, since $M_2 \sim n_i^6$ [30–32], for these crystals, one can expect a higher AO efficiency than for other crystals of the LGS group, as well as a higher efficiency in terms of path difference, which can be used in polarization-optical light modulators and, accordingly, pressure sensors based on them [33–36].

In papers [24,37,38] quantum–mechanical calculation of POCs and ELOCs for a number of crystals using the CRYSTAL program [39] ensured good agreement with experimental data. Here, the calculation of photoelastic constants of BTGS crystals was also carried out using version CRYSTAL17 of this program [40]. The program implements automated algorithms for determination of elastic and piezoelectric [41], piezo-optic and elasto-optic [42] tensors for crystals of any symmetry. The hybrid PBE0 functional of the density functional theory (DFT) is used [43], which is known to provide accurate strain-related properties of solids [44–46]. The POB-TZVP-rev2 atom-centered Gaussian-type function basis set has been adopted for all elements [47,48]. The integration was performed on a $5 \times 5 \times 5$ k-grid chosen by the Monkhrost-Pack method. Convergence of the self-consistent field step of the calculations is determined by a threshold on the energy set to 10^{-8} Hartree.

3. Results and Discussion

3.1. Elastic and Photoelastic Coefficients

BTGS crystals belong to the point group 32 [2] and, accordingly, have seven independent coefficients of elastic stiffness C_{mk} and elastic compliance S_{km}, as well as eight independent elasto-optic p_{ik} and piezo-optic π_{im} coefficients [49,50]. The calculated values of elastic C_{mk}, S_{km} and photoelastic p_{ik}, π_{im} coefficients for these crystals are indicated in Tables 1 and 2.

Table 1. Elastic coefficients C_{mk} (10^9 N/m^2) and S_{km} (10^{-12} m$_2$/N) of BTGS crystals calculated by quantum–mechanical technique (in comparison with literature data).

C_{mk}	C_{11}	C_{12}	C_{13}	C_{33}	C_{14}	C_{44}
[22]	166.0	–	–	–	6.3	–
[51] **	160.5	77.4	85.5	170.9	3.03	63.3
Our data	164.9	72.0	83.6	192.0	–6.38	66.3
S_{km}	S_{11}	S_{12}	S_{13}	S_{33}	S_{14}	S_{44}
[51] *	9.32	−2.75	−3.28	9.14	0.58	15.85
Our data	8.50	−2.41	−2.65	7.50	1.05	15.28

* The symbol (*) denotes experimentally obtained results; the symbol (**) denotes C_{mk} coefficients calculated based on the known relation $C_{mk} = S_{km}{}^{-1}$ and experimentally determined S_{km}.

Table 2. Piezo-optic π_{im} (in units of 10^{-12} m^2/N = Br = Brewster) and elasto-optic p_{ik} coefficients of BTGS crystals calculated by the quantum–mechanical technique.

π_{11}	π_{12}	π_{13}	π_{31}	π_{33}	π_{14}	π_{41}	π_{44}
−0.18	0.65	0.78	1.31	−1.48	0.26	0.11	−0.46
p_{11}	p_{12}	p_{13}	p_{31}	p_{33}	p_{14}	p_{41}	p_{44}
0.08	0.162	0.189	0.185	−0.067	0.023	0.013	−0.032

As seen from Table 1, the agreement between the calculated (our data) and experimental [22,51] values of the elastic coefficients C_{mk} and S_{km} is mostly good. Further, these coefficients were used for calculation of the AO efficiency and constructing extreme surfaces of the change in the optical path difference $\delta\Delta_k$ between orthogonally polarized beams induced by the uniaxial pressure σ_m.

The highest value of POCs for BTGS crystals (Table 2) corresponds to the coefficient π_{33}, as for other studied crystals of the LGS group [18–20]. For ELOCs, we see that the highest coefficients are p_{13} and p_{31}, so the transverse effect prevails, as in CTGS [19] and CGG [20]. Let us pay attention to an interesting observation: if the values of the POE and ELOE in crystals of the LGS group are related to the crystal lattice parameters, then larger photoelastic effects are generally observed in CTGS [12,19], LGS [18] and BTGS crystals with a larger unit cell volume (V = 283.80 Å^3 [52], 294.28 Å^3 [53] and 326.03 Å^3 [2], respectively) compared to the small value of V = 279.96 Å^3 [54] for CGG crystals and, accordingly, the predominantly smaller values of POCs and ELOCs for this crystal [20]. It was also found that the maximum values of POE or ELOE are sensitive to the ratio of the cell parameters c/a. Namely, in the LGS crystal with a higher value of c/a = 0.6233 [55], longitudinal effects corresponding to the coefficients π_{33} and p_{33} [18] predominate, while in BTGS, CTGS and CGG crystals with smaller values of the c/a ratio (0.6097, 0.6148 and 0.6158, respectively [2,52,54]), transverse effects with the coefficients π_{i31}, p_{13} and p_{31} [18–20] are more significant.

Note that crystals of the LGS group are often divided into ordered and disordered, see, e.g., papers [10,22,54,55]. If, according to the piezoelectric coefficients, there is a large difference between ordered crystals (e.g., CTGS, CNGS) and disordered ones (e.g., LGS, LGT) [10,11], then no clear patterns have been found for the photoelastic coefficients π_{im}, p_{ik}. We can only note that for crystals with an ordered structure (CTGS, CNGS, BTGS) transverse elasto-optic effects prevail (i.e., the coefficients p_{13}, p_{31} are larger), whereas for crystals with a disordered structure (LGS, CGG), similar patterns have not been revealed for either ELOE or POE.

3.2. Evaluation of Acousto-Optic Efficiency

Let us estimate the value of the AO figure-of-merit of BTGS crystal based on the known [30–32] expression

$$M_2 = \frac{n_i^6 p_{ik}^2}{\rho V_k^3}, \tag{2}$$

where ρ is the crystal density and V_k is the acoustic wave velocity.

For the conditions of AO interaction with a longitudinal acoustic wave, which correspond to the maximum ELOC p_{31} = 0.185 (Table 2), expression (2) should be substituted with this value of p_{31}. At refractive index n_3 = 1.8776 (for the wavelength of 632.8 nm [29]), the velocity of the longitudinal acoustic wave V_3 = 5908 m/s, calculated by the Christoffel method [50] based on the elasticity coefficients C_{mk} (Table 1), and the density of BTGS crystal ρ = 5514 kg/m^3 [2] were used. The result is $M_2 = 1.66 \cdot 10^{-15}$ s^3/kg. In terms of this M_2 value, BTGS crystal is approximately two times superior to the strontium borate (SrB_4O_7) crystal, suitable for AO modulation of light in the ultraviolet range [56] and has a value comparable to the maximum of M_2 of the CTGS crystal [19]. However, to find the maximum AO efficiency of BTGS crystal, it is necessary to construct AO figure-of-merit (M_2) surfaces and analyze the anisotropy of these surfaces using the technique described, e.g., in [28].

3.3. Extreme Piezo-Optic Surfaces of the Path Difference

The path difference POE $\delta\Delta_k$ according to expression (1) consists of changing the birefringence Δn_k and the sample thickness d_k under the influence of mechanical stress σ_m. Such POE finds its application in polarization-optical light modulators, particularly, in pressure gauges based on them [33–36]. We call such surfaces extreme, because each point of the surface is obtained not simply as a result of calculation using a known expression, but as a consequence of optimization (searching for the maximum path difference in accordance with the direction of uniaxial pressure applying or light wave vector). This optimization is based on the well-known classical Levenberg–Marquardt algorithm [57]. To avoid the uncertainty caused by reaching a local maximum, the search was performed several times for each point of the surface, with 10 different initial values for each optimization parameter (i.e., the polar or azimuthal angle of the spherical coordinate system). It should also be noted that the calculations for each point of the surface were carried out independently, and reaching a local (non-global) maximum in such a case is usually reflected in the shape of the extreme surface and violates its symmetry caused by the symmetry of the crystal, or forms 'dips' on the surface. Such situations are easily traced; however, they were not encountered in the calculations of this work. The construction of extreme surfaces of the path difference is detailed, particularly, in [27].

Here the objective function of optimization is the absolute value of π'^{o}_{km} corresponding to the definition of POE by path difference [58]:

$$\pi'^{o}_{km} = 2\frac{\delta(\Delta n_k \cdot d_k)}{\sigma_m d_k}. \tag{3}$$

Based on this expression, we obtain the equation of the π'^{o}_{km} surface, which describes the change in the path difference for all directions $\vec{m}$ of the applied uniaxial pressure and all light propagation directions $\vec{k}$, namely

$$\pi'^{o}_{km} = \pi'_{im}(n'_i)^3 - \pi'_{jm}(n'_j)^3 - 2\Delta n'_k \cdot S'_{km}, \quad (4)$$

where the dashes indicate the spatial distribution of all effects: π'^{o}_{km} is POE in terms of the path difference; π'_{im} and π'_{jm} are POEs consisting refractive indices of orthogonally polarized waves n'_i and n'_j changes; $\Delta n'_k$ is the birefringence; is the effective elastic compliance coefficient. It should be emphasized that all possible geometries of piezo-optic interaction were considered, and not only the conditions of orthogonality of $\vec{k}$ and $\vec{m}$ directions.

The calculation by the method of extreme surfaces (see, e.g., [27,28]) was carried out in two equivalent variants. In the first variant of the calculation, for each possible direction $\vec{k}$ of light propagation, such a direction $\vec{m}$ of uniaxial pressure σ_m was determined, which would provide the maximum of the path difference π'^{o}_{km}. The dependence of the obtained maximum values π'^{o}_{km} on the direction $\vec{k}$ of the light wave can be represented in the form of a surface, which we call the wave vector extreme surface. The distances of the points of this surface from the origin of coordinates correspond to the absolute values of the maximum π'^{o}_{km} for each direction of the wave vector $\vec{k}$. Among all π'^{o}_{km} maxima obtained as a result of the calculation, the global maxima of this value were determined, which correspond to the maximum achievable POE of the path difference. In the second variant of the calculation, for each possible direction $\vec{m}$ of uniaxial pressure, such a direction of wave vector $\vec{k}$ was determined, which would also provide the maximum of π'^{o}_{km} surface. The corresponding extreme surface is called the surface of mechanical stress. Both types of surfaces have all the symmetry elements of the point group of the crystal and the center of inversion (i.e., they correspond to the Laue group of the crystal [59]). The symmetry reveals in the existence of few equivalent global maxima. Although the wave vector and mechanical stress surfaces differ in form, the maximum achievable global maxima of the POE must be the same for both of them.

Parameters of LGS, CGG, CTGS, CNGS and BTGS crystals (π_{im}, S_{km}, n_i) used for construction of extreme surfaces π'^{o}_{km} were taken from [18–20,24,29] and Tables 1 and 2.

The examples of the extreme surfaces of the POE by the path difference, constructed in accordance with (4), are shown in Figures 1 and 2. The results of the optimization for the experimentally studied (by interferometric method) crystals CGG [20], CTGS [19] and LGS [18] and the theoretically studied (by quantum–mechanical method) crystals CTGS [24], CNGS [24] and BTGS (this paper) are indicated in Tables 3 and 4. These tables provide data on the position of one of the global maxima, the positions of other ones can be determined using the symmetry elements of the point group 32 supplemented by inversion in accordance with the symmetry of the expressions used for calculations (specifically, the use of the absolute value of π'^{o}_{km} as the objective function).

As seen from Table 3, for CGG and CTGS crystals, the maximum values of the π'^{o}_{km} surfaces were obtained for the case of orthogonal conditions of piezo-optic interaction ($\alpha = 90°$), when the direction $\vec{m}$ of pressure applying coincides with the main crystallographic axis X, and light propagates in the main crystallographic plane YZ in directions determined by the angles $\theta_k = 104°$ and $101.3°$ to the optical axis Z of the considered crystals. For LGS crystal, the most effective geometry of piezo-optic interaction corresponds to the case when the light propagates and the uniaxial pressure is applied in the crystallographic plane YZ. The optimal geometry of interaction is not strictly orthogonal, the angle α is

equal to 95.5°. The smallest global value of POE by the path difference π'^{o}_{km} is obtained for CGG crystal (Table 3). This result is obviously caused by the values of the refractive indices n_i, birefringence Δn_k and piezo-optic coefficients π_{im} of this crystal, which are lower compared to other representatives of the langasite group [20].

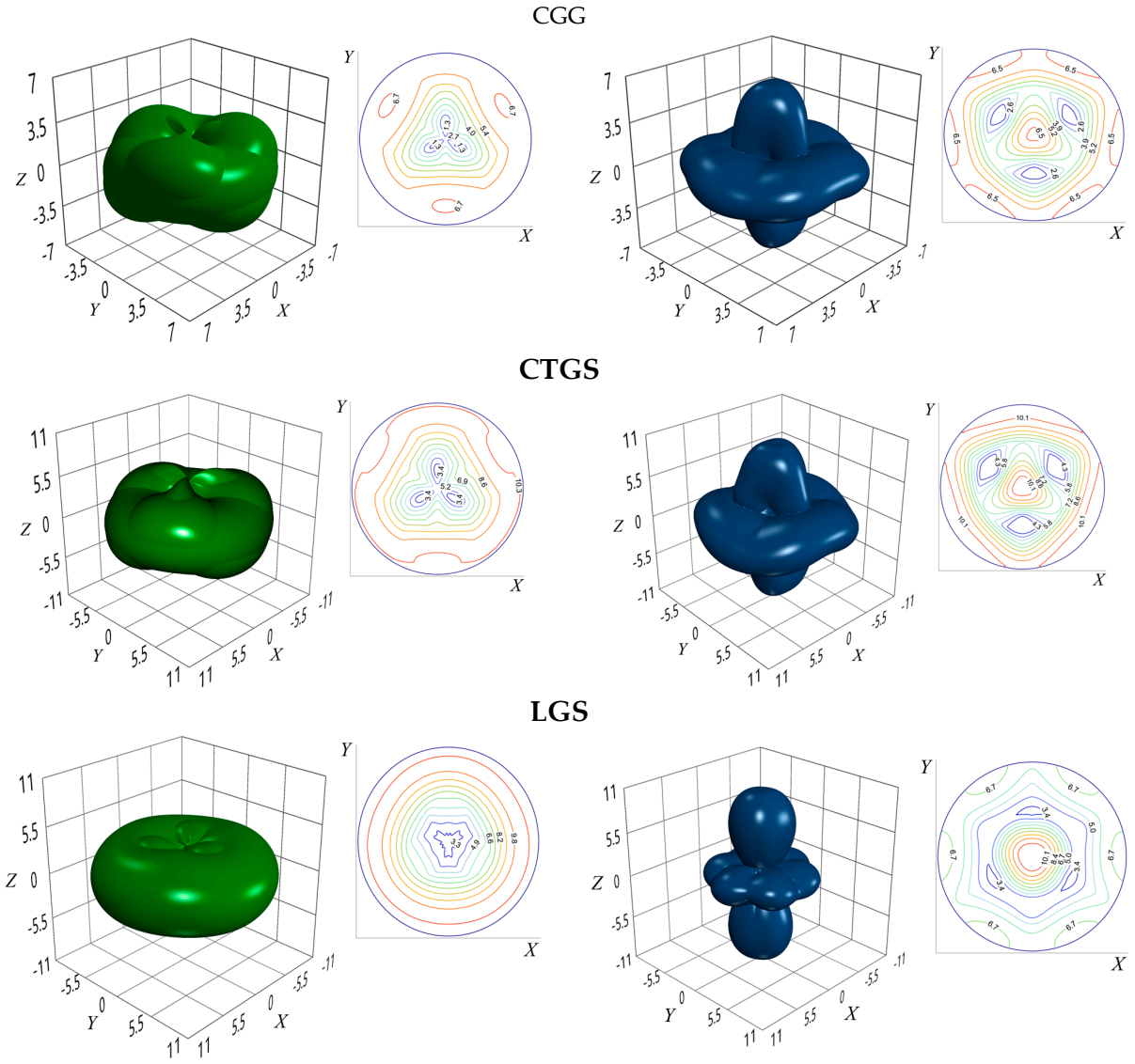


Figure 1. The extreme surfaces π'^{o}_{km} of the wave vector (**left**) and mechanical stress (**right**) for CGG, CTGS and LGS crystals; the inserts show the stereographic projections of the surfaces. The optimization is based on the experimental data; all values are in Br (10^{-12} m^2/N).

It should be emphasized that Figures 1 and 2 give a qualitative representation of the anisotropy of the POE in terms of the path difference, whereas Tables 3 and 4 present quantitative results of the maximum (global) values of the piezo-optic extreme surfaces of the path difference.

The most important results presented in Tables 3 and 4 include the following:

(1) The directions of light propagation $\vec{k}$ indicated in these tables do not correspond to the main crystallographic axes (an exception exists only for BTGS crystal, see rows 4 and 5 in Table 4); the directions of light propagation $\vec{k}$ and uniaxial pressure applying $\vec{m}$ are either strictly orthogonal ($\alpha = 90°$, see rows 1 and 2 in Table 3 and rows 1 and 5 in Table 4), or deviate from orthogonality by small angles from 2.4° to 5.5° (see row 3 in Table 3 and rows 2–4 in Table 4);

(2) Among the experimentally and theoretically studied crystals, the maximal value of π'^{o}_{km} was obtained for BTGS crystal (14.5 Br);
(3) CGG crystal reveals the lowest global maximum of π'^{o}_{km} (6.8 Br); for comparison, the maximum value of the POE (in terms of path difference) for quartz found by the extreme surface method is equal to 7.4 Br, which is also significantly (by a factor of 2) lower than that for BTGS crystal (Table 4). Therefore, it is BTGS crystals that should be preferred when using them as sensitive elements of polarization-optic light modulators and devices based on them.

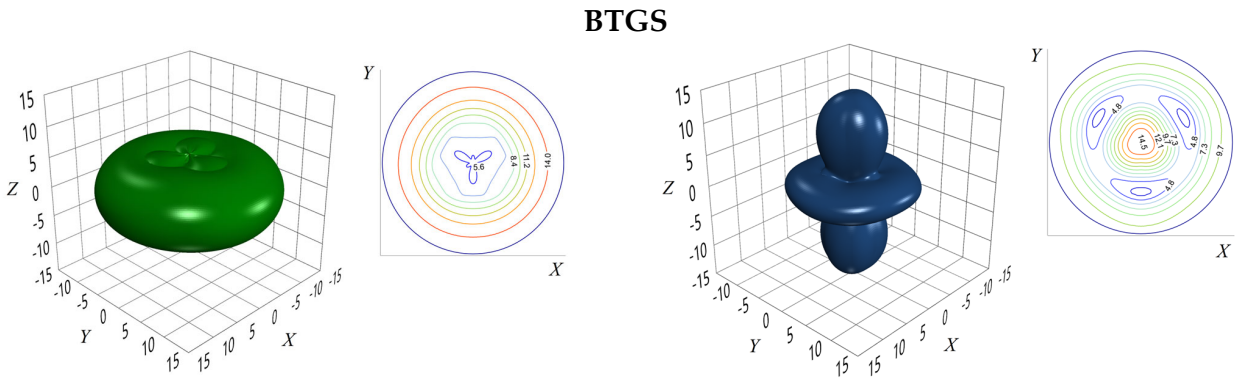


Figure 2. The extreme surfaces π'^{o}_{km} of the wave vector (**left**) and mechanical stress (**right**) for BTGS crystal; the inserts show the stereographic projections of the surfaces. The optimization is based on the data obtained by quantum–mechanical method; all values are in Br.

Table 3. Maximal values and angle parameters for the extreme surfaces of POE π'^{o}_{km} in CGG, CTGS and LGS crystals; the optimization is based on the experimental data.

Crystal	Light Wave				Direction of Uniaxial Pressure Applying		α, deg.	The Global Maximum, Br
	θ_k, deg.	φ_k, deg.	θ_i, deg.	φ_i, deg.	θ_m, deg.	φ_m, deg.		
CGG	104	90	90 (*o*), 14 (*e*)	0 (*o*), 90 (*e*)	90	0	90	6.8
CTGS	101.3	90	90 (*o*), 11.3 (*e*)	0 (*o*), 90 (*e*)	90	0	90	10.4
LGS	91	90	90 (*o*), 1 (*e*)	0 (*o*), 90 (*e*)	−4.5	90	95.5	10.8

Hereinafter θ_k, φ_k, θ_i, φ_i, θ_m and φ_m are the angles of spherical coordinate system for the directions of wave $\vec{k}$, light polarization $\vec{i}$ and the direction of uniaxial pressure applying $\vec{m}$. This spherical coordinate system is connected with the crystal-physics Cartesian coordinate system *X*, *Y*, *Z*; the designations (*o*) and (*e*) correspond to the polarization directions of the ordinary and extraordinary beams, respectively, α is the angle between $\vec{k}$ and $\vec{m}$ vectors.

Table 4. Maximal values and angle parameters for the extreme surfaces of POE π'^{o}_{km} in CTGS, CNGS and BTGS crystals; the optimization is based on the data obtained by quantum–mechanical method.

Crystal	Light Wave				Direction of Uniaxial Pressure Applying		α, deg.	The Global Maximum, Br
	θ_k, deg.	φ_k, deg.	θ_i, deg.	φ_i, deg.	θ_m, deg.	φ_m, deg.		
CTGS	124	90	90 (*o*), 35 (*e*)	0 (*o*), 90 (*e*)	90	0	90	11.0
	155	90	90 (*o*), 65 (*e*)	0 (*o*), 90 (*e*)	60	90	95	11.0
CNGS	146.4	90	90 (*o*), 56.4 (*e*)	0 (*o*), 90 (*e*)	52	90	94.4	11.6
BTGS	90	90	90 (*o*), 0 (*e*)	0 (*o*), 0 (*e*)	2.4	90	87.6	14.5
	90	90	90 (*o*), 0 (*e*)	0 (*o*), 0 (*e*)	90	0	90	14.5

4. Conclusions

All elastic and photoelastic (piezo-optic and elasto-optic) coefficients of BTGS crystals were calculated using the quantum–mechanical method realized in the CRYSTAL17 program. Based on the calculated elastic compliance coefficients S_{km} and piezo-optic coefficients π_{im}, as well as the known values of the refractive indices n_i for the light wavelength λ = 632.8 nm, extreme surfaces of the POE π'^{o}_{km} were constructed, which describe the spatial distribution of the change in the path difference $\delta\Delta_k$ caused by the influence of the mechanical stress σ_m. The maximum (global) values of the piezo-optic extreme surfaces of the path difference were found by the Levenberg–Marquardt method. The results obtained for BTGS crystals are compared with the ones for other crystals of the langasite group: LGS, CGG, CTGS and CNGS. The main result of the research is that the BTGS crystal reveals the highest value of the POE π'^{o}_{km} among all studied crystals of langasite group (14.5 Br). This value is significantly (twice) higher than the one for quartz (7.4 Br). Therefore, BTGS crystals should be preferred when used as sensitive elements of polarization-optic light modulators and devices based on them.

The value of the AO figure-of-merit M_2 of BTGS crystal was estimated based on the highest elasto-optic coefficient p_{31}. According to the obtained value of $M_2 = 1.66 \cdot 10^{-15}$ s^3/kg, BTGS crystal is twice as much as the strontium borate crystal (SrB_4O_7), which is suitable for acousto-optic modulation of light in the ultraviolet range.

It should be emphasized that for the studied crystals, a correlation was found between the value of the piezo-optic π_{im} and elasto-optic p_{ik} coefficients on the one hand and the volume of the crystal lattice on the other. Moreover, the values of the π_{im} and p_{ik} coefficients correlate with the value of the ratio of the unit cell parameters c/a.

It was also found that for crystals with an ordered structure (CTGS, CNGS, BTGS), the transverse elasto-optic effects (corresponding to the coefficients p_{13}, p_{31}) prevail, and for crystals with a disordered structure (LGS, CGG), similar regularities were not determined for either ELOE or POE.

Based on the results obtained, it can be stated that by changing the parameters of the unit cell by incorporating the appropriate cations in the crystal structure, the photoelastic properties of crystals of the langasite group can be controlled. For example, replacing the Ca^{2+} cation with Ba^{2+} in crystals with an ordered structure (CTGS, BTGS) leads to a significant increase in the maximum POE value by the path difference π'^{o}_{km} (by about 50%), namely, from 10.4 Br for CTGS to 14.5 Br for BTGS.

It is clear that before developing recommendations for the practical use of an effective (based on quantum–mechanical calculation) photoelastic material, a thorough experimental verification (by interferometry methods) of the calculated values of POCs and ELOCs should be carried out. In other words, the method of quantum–mechanical calculation should be considered as an effective express technique for the initial assessment of the photoelastic characteristics of considered crystals.

Author Contributions: Conceptualization, B.M.; methodology, N.D. and O.B.; software, O.B. and P.S.; validation, B.M.; formal analysis, A.A.; investigation, N.D., B.M., O.B., P.S. and O.L.; writing—original draft preparation, N.D.; writing—review and editing, B.M.; visualization, P.S.; supervision, B.M. and A.A.; project administration, B.M. and A.A. All authors have read and agreed to the published version of the manuscript.

Funding: This research has received funding from the Ministry of Education and Science of Ukraine in the frames of 'Nanoelectronics' (0123U101695). We acknowledge the support of the European Union under Horizon Europe for the TeraHertz project (Grant Agreement 101086493).

Data Availability Statement: All data generated or analyzed during this study are included in this published article.

Conflicts of Interest: The authors declare no conflicts of interest.

References

1. Remark, T.; Segonds, P.; Debray, J.; Jegouso, D.; Víllora, E.; Shimamura, K.; Boulanger, B. Linear and nonlinear optical properties of the langasite crystal $Ca_3TaAl_3Si_2O_{14}$. *Opt. Mater. Expr.* **2023**, *13*, 2053–2060. [CrossRef]
2. Usui, H.; Kusakabe, H.; Tokuda, M.; Sugiyama, K.; Hoshina, T.; Tsurumi, T.; Takeda, H. Structure and electrical properties of $Ba_3TaGa_3Si_2O_{14}$ single crystals grown by Czochralski method. *J. Ceram. Soc. Jpn.* **2020**, *128*, 441–446. [CrossRef]
3. Kuzmin, N.; Klimin, S.; Mavrin, B.; Boldyrev, K.; Chernyshev, V.; Mill, B.; Popova, M. Lattice dynamics and structure of the new langasites $Ln_3CrGe_3Be_2O_{14}$ (Ln = La, Pr, Nd): Vibration alspectra and abinitio calculations. *J. Phys. Chem. Solids* **2020**, *138*, 109266. [CrossRef]
4. Golovina, T.; Konstantinova, A.; Zabelina, E.; Kozlova, N.; Kasimova, V. Allowance for the imperfection of the spectrophotometric complex optical elements when measuring transmission spectra of gyrotropic uniaxial crystals. I: Samples are cut perpendicular to the optical axis. *Cryst. Rep.* **2025**, *70*, 39–49. [CrossRef]
5. Deng, M.; Chen, J.; Zhang, J.; Xie, W.; Jin, H.; Xuan, W.; Dong, S.; Luo, J. Numerical design and optimization of high performance Langasite and hetero-acoustic layer-based surface acoustic wave device. *Micromachines* **2025**, *16*, 166. [CrossRef]
6. Roshchupkin, D.; Kovalev, D. Coefficients of thermal expansion in $La_3Ga_5SiO_{14}$ and $Ca_3TaGa_3Si_2O_{14}$ crystals. *Materials* **2023**, *16*, 4470. [CrossRef]
7. Andreev, I. Two decades following the discovery of thermallys table elastic properties of $La_3Ga_5SiO_{14}$ crystal and coining of the term langasite. *Tech. Phys.* **2004**, *49*, 1101–1103. [CrossRef]
8. Andreev, I.; Dubovik, M. A new piezoelectric material, langasite ($La_3Ga_5SiO_{14}$), with a zero temperature coefficient of the elastic vibration frecuency. *Sov. Tech. Phys. Lett.* **1984**, *10*, 205–207.
9. Fu, X.; Villora, E.; Matsushita, Y.; Kitanaka, Y.; Noguchi, Y.; Miyayama, M.; Shimamura, K.; Ohashi, N. Influence of growth conditions on the optical, electrical resistivity and piezoelectric properties of $Ca_3TaGa_3Si_2O_{14}$ single crystals. *J. Ceram. Soc. Jpn.* **2016**, *124*, 523–527. [CrossRef]
10. Irzhak, D.; Roshchupkin, D. Piezoelectric strain coefficients in $La_3Ga_{5.3}Ta_{0.5}Al_{0.2}O_{14}$ and $Ca_3TaGa_3Si_2O_{14}$ crystals. *AIP Adv.* **2013**, *3*, 102108. [CrossRef]
11. Irzhak, D.; Roshchupkin, D. Measurement of independent piezoelectric moduli of $Ca_3NbGa_3Si_2O_{14}$, $La_3Ga_{5.5}Ta_{0.5}O_{14}$ and $La_3Ga_5SiO_{14}$ single crystals. *J. Appl. Cryst.* **2018**, *51*, 1174–1181. [CrossRef]
12. Fritze, H. High-temperature bulk acoustic wave sensors. *Meas. Sci. Technol.* **2011**, *22*, 012002. [CrossRef]
13. Xin, Y.; Shaojun, Z.; Jiyang, W. Mutualaction of the opticalactivity and the electro-optic effect and itsinf luence on the $La_3Ga_5SiO_{14}$ crystal electro-optic *Q* switch. *J. Opt. Soc. Am. B* **2005**, *22*, 394–397. [CrossRef]
14. Zhang, J.; Tan, Q.; Zhang, L.; Zhao, N.; Liang, X. Langasite bonding via high temperature for fabricating sealed microcavity of pressure sensors. *Micromachines* **2022**, *13*, 479. [CrossRef] [PubMed]
15. Kong, H.; Wang, J.; Zhang, H.; Yin, X.; Zhang, S.; Liu, Y.; Cheng, X.; Gao, L.; Hu, X.; Jiang, M. Growth, properties and application as an electrooptic Q-switch of langasite crystal. *J. Cryst. Growth* **2003**, *254*, 360–367. [CrossRef]
16. Boursier, E.; Segonds, P.; Boulanger, B.; Félix, C.; Debray, J.; Jegouso, D.; Ménaert, B.; Roshchupkin, D.; Shoji, I. Phase-matching directions, refined sellmeier equations, and second-order nonlinear coefficient of the infrared langatate crystal $La_3Ga_{5.5}Ta_{0.5}O_{14}$. *Opt. Lett.* **2014**, *39*, 4033–4036. [CrossRef]
17. Boursier, E.; Giedre, M.; Delagnes, J.-C.; Petit, S.; Ernotte, G.; Lassonde, P.; Segonds, P.; Boulanger, B.; Petit, Y.; Légaré, F.; et al. Study of middle infrared difference frequency generation using a femtosecond laser source in LGT. *Opt. Lett.* **2017**, *42*, 3698–3701. [CrossRef]
18. Mytsyk, B.; Demyanyshyn, N.; Andrushchak, A.; Kost', Y.; Parasyuk, O.; Kityk, A. Piezooptical coefficients of $La_3Ga_5SiO_{14}$ and $CaWO_4$ crystals: A combined optical interferometry and polarization-optical study. *Opt. Mater.* **2010**, *33*, 26–30. [CrossRef]
19. Mytsyk, B.; Suhak, Y.; Demyanyshyn, N.; Buryy, O.; Syvorotka, N.; Sugak, D.; Ubizskii, S.; Fritze, H. Full set of piezo-optic and elasto-optic coefficients of $Ca_3TaGa_3Si_2O_{14}$ crystals at room temperature. *Appl. Opt.* **2020**, *59*, 8951–8958. [CrossRef]
20. Mytsyk, B.; Demyanyshyn, N.; Andrushchak, A.; Maksishko, Y.; Kohut, Z.; Kityk, A. Characterization of photoelastic materials by Mach-Zehnder interferometry: Application to trigonal calcium galogermanate (CGG) crystals. *J. Appl. Phys.* **2024**, *135*, 085111. [CrossRef]
21. Chani, V.; Shimamura, K.; Yu, Y.; Fukuda, T. Design of newoxidecrystals with improved structural stability. *J. Mater. Sci. Eng.* **1997**, *20*, 281–338. [CrossRef]
22. Zheng, Y.; Cui, S.; Chen, J.; Tu, X.; Xin, J.; Kong, H.; Shi, E. *Advances in design, growth and application of piezoelectric crystals with langasite structure. Proc. 2012 Symposium on Piezoelectricity, Acoustic Waves, and Device Applications (SPAWDA), Shanghai, China, 23–25 November 2012*; IEEE Xplore: Piscataway, NJ, USA, 2013; pp. 252–259.
23. Mytsyk, B.; Kryvyy, T.; Demyanyshyn, N.; Mys, O.; Martynyuk-Lototska, I.; Kokhan, O.; Vlokh, R. Piezo-, elasto- and acousto-optic properties of Tl_3AsS_4 crystals. *Appl. Opt.* **2018**, *57*, 3796–3801. [CrossRef]

24. Mytsyk, B.; Erba, A.; Maul, J.; Demyanyshyn, N.; Shchepanskyi, P.; Syrotynsky, O. Photoelasticity of CNGS crystals. *Appl. Opt.* **2023**, *62*, 7952–7959. [CrossRef]
25. Mytsyk, B.; Demyanyshyn, N. Piezooptic surfaces of lithium niobate crystals. *Crystallogr. Rep.* **2006**, *51*, 653–660. [CrossRef]
26. Mytsyk, B.; Andrushchak, A. Spatial distribution of the longitudinal and transverse piezooptical effect in lithium tantalate crystals. *Crystallogr. Rep.* **1996**, *41*, 1001–1006.
27. Buryy, O.; Demyanyshyn, N.; Mytsyk, B.; Andrushchak, A. Optimization of the piezooptic interaction geometry in SrB_4O_7 crystal. *Opt. Applik.* **2016**, *XLVI*, 447–459.
28. Buryy, O.; Demyanyshyn, N.; Mytsyk, B.; Andrushchak, A.; Sugak, D. Acousto-optic interaction in LGS and CTGS crystals. *Opt. Contin.* **2022**, *1*, 1314–1323. [CrossRef]
29. Konstantinova, A.; Golovina, T.; Nabatov, B.; Dudka, A.; Mill, B. Experimental and theoretical determination of the optical rotation in langasite family crystals. *Crystallogr. Rep.* **2015**, *60*, 907–914. [CrossRef]
30. Pinnow, D.; Van, G.; Warner, A.; Bonner, W. Lead molybdate: A melt-grown crystal with a high figure of merit for acousto-optic device applications. *Appl. Phys. Lett.* **1969**, *15*, 83–86. [CrossRef]
31. Dixon, R. Photoelastic properties of selected materials and their relevance for applications to acoustic light modulators and scanners. *J. Appl. Phys.* **1967**, *38*, 5149–5153. [CrossRef]
32. Uchida, N.; Niizeki, N. Acoustooptic deflection materials and techniques. *Proc. IEEE* **1973**, *61*, 1073–1092. [CrossRef]
33. Spillman, W.B., Jr. Multimode fiber-optic pressure sensor based on the photoelastic effect. *Opt. Lett.* **1982**, *7*, 388–390. [CrossRef]
34. Trainer, N. Photoelastic Measuring Transducer and Accelerometer Based Thereon. U.S. Patent 4,648,273, 10 March 1987.
35. Andrushchak, A.; Mytsyk, B.; Osyka, B. Polarized-optical pressure meter. *Devices Tech. Exp.* **1990**, *3*, 241. (In Russian)
36. Wang, B. Linear birefringence measurement instrument using two photoelastic modulators. *Opt. Eng.* **2000**, *41*, 981–987. [CrossRef]
37. Erba, A.; Ruggiero, M.; Korter, T.; Dovesi, R. Piezo-optic tensor of crystals from quantum-mechanical calculations. *J. Chem. Phys.* **2015**, *143*, 144504. [CrossRef]
38. Demyanyshyn, N.; Mytsyk, B.; Andrushchak, A.; Kityk, A. Photoelasticity of crystals with the scheelite structure: Quantum mechanical calculations. *Acta Crystallogr. Sect. B* **2025**, *B81*, 47–54. [CrossRef] [PubMed]
39. Perger, W.; Criswell, J.; Civalleri, B.; Dovesi, R. Ab-initio calculation of elastic constants of crystalline systems with the CRYSTAL code. *Comput. Phys. Commun.* **2009**, *180*, 1753–1759. [CrossRef]
40. Dovesi, R.; Erba, A.; Orlando, R.; Zicovich-Wilson, C.; Civalleri, B.; Maschio, L.; Rèrat, M.; Casassa, S.; Baima, J.; Salustro, S.; et al. Quantum-mechanical condensed matter simulations with CRYSTAL. *WIREs Comput. Mol. Sci.* **2018**, *8*, e1360. [CrossRef]
41. Erba, A.; Caglioti, D.; Zicovich-Wilson, C.; Dovesi, R. Nuclear-relaxed elastic and piezoelectric constants of aterials: Computational aspects of two quantum-mechanical approaches. *J. Comput. Chem.* **2017**, *38*, 257–264. [CrossRef]
42. Erba, A.; Dovesi, R. Photoelasticity of crystals from theoretical simulations. *Phys. Rev.* **2013**, *B88*, 045121. [CrossRef]
43. Adamo, C.; Barone, V. Toward reliable density functional methods without adjustable parameters: The PBE0 model. *J. Chem. Phys.* **1999**, *110*, 6158–6170. [CrossRef]
44. Mahmoud, A.; Erba, A.; El-Kelany, K.; Rérat, M.; Orlando, R. Low-temperature phase of $BaTiO_3$: Piezoelectric, dielectric, elastic and photoelastic properties from ab initio simulations. *Phys. Rev.* **2014**, *B89*, 045103. [CrossRef]
45. El-Kelany, K.; Carbonnière, P.; Erba, A.; Rérat, M. Inducing a finite in-plane piezoelectricity in graphene with low concentration of inversion symmetry-breaking defects. *J. Phys. Chem. C* **2015**, *119*, 8966–8973. [CrossRef]
46. El-Kelany, K.; Carbonnière, P.; Erba, A.; Sotiropoulos, J.-M.; Rérat, M. Piezoelectricity of functionalized graphene: A quantum mechanical rationalization. *J. Phys. Chem. C* **2016**, *120*, 7795–7803. [CrossRef]
47. Laun, J.; Bredow, T. BSSE-corrected consistent Gaussian basis sets of triple-zeta valence with polarization quality of the sixth period for solid-state calculations. *J. Comput. Chem.* **2021**, *42*, 1064–1072. [CrossRef] [PubMed]
48. Laun, J.; Bredow, T. BSSE-corrected consistent Gaussian basis sets of triple-zeta valence with polarization quality of the fifth period for solid-state calculations. *J. Comput. Chem.* **2022**, *43*, 839–846. [CrossRef]
49. Nye, J.F. *Physical Properties of Crystals*; Oxford: Clarendon Press: Oxford, UK, 1964.
50. Narasimhamurty, T. *Photoelastic and Electro-Optic Properties of Crystals*; Plenum Press: New York, NY, USA; London, UK, 1981.
51. Dudka, A. Ab Initio calculation of elastic and electromechanical constants of langasite family crystals. *Crystallogr. Rep.* **2012**, *57*, 131–133. [CrossRef]
52. Wang, Z.; Yu, W.; Yuan, D.; Wang, X.; Xue, G.; Shi, X.; Xu, D.; Lv, M. Crystal structure of tricacium tantalum trigallium disilicon oxide, $Ca_3TaGa_3Si_2O_{14}$. *Z. Für Krist.—New Cryst. Struct.* **2003**, *218*, 389–390.
53. Dudka, A. New multicell model for describing the atomic structure of $La_3Ga_5SiO_{14}$ piezoelectric crystal: Unitcells of different compositions in the same single crystal. *Crystallogr. Rep.* **2017**, *62*, 195–204. [CrossRef]
54. Dudka, A.; Mill, B. Accurate crystal-structure refinement of $Ca_3Ga_2Ge_4O_{14}$ at 295 and 100 K and analysis of the disorder in the atomic positions. *Crystallogr. Rep.* **2013**, *58*, 594–603. [CrossRef]

55. Chait, B.; Bustamante, A.; Chout, M. A new class of ordered langasite structure compound. In Proceedings of the 2000 IEEE/EIA International Frequency Control Symposium and Exhibition (Cat. No.00CH37052), New York, NY, USA, 9 June 2000; pp. 163–168.
56. Mytsyk, B.; Demyanyshyn, N.; Martynyuk-Lototska, I.; Vlokh, R. Piezo-optic, photoelastic, and acousto-optic properties of SrB_4O_7 crystals. *Appl. Opt.* **2011**, *50*, 3889–3895. [CrossRef] [PubMed]
57. Press, W.; Teukolsky, S.; Vetterling, W.; Flannery, B. *Numerical Recipes in C. The Art of Scientific Computing*, 2nd ed.; Cambridge University Press: Cambridge, UK, 1992.
58. Mytsyk, B. Methods for the studies of the piezo-optical effect in crystals and the analysis of experimental data. I. Methodology for the studies of piezo-optical effect. *Ukr. J. Phys. Opt.* **2003**, *4*, 1–26. [CrossRef] [PubMed]
59. Sirotin, Y.; Shaskolskaja, M. *Fundamentals of Crystal Physics*; Mir Publishers: Moscow, Russia, 1982.

Disclaimer/Publisher's Note: The statements, opinions and data contained in all publications are solely those of the individual author(s) and contributor(s) and not of MDPI and/or the editor(s). MDPI and/or the editor(s) disclaim responsibility for any injury to people or property resulting from any ideas, methods, instructions or products referred to in the content.